A99-16665

AIAA 99-0816
Effect of Total Temperature on Boundary Layer Stability at Mach 6

R. L. Kimmel and J. Poggie
Air Force Research Laboratory
Air Vehicles Directorate
Wright-Patterson AFB, OH

37th AIAA Aerospace Sciences Meeting and Exhibit
January 11-14, 1999 / Reno, NV

EFFECT OF TOTAL TEMPERATURE ON BOUNDARY LAYER STABILITY AT MACH 6

Roger L. Kimmel*
Jonathan Poggie†
U. S. Air Force Research Laboratory
Air Vehicles Directorate
Wright-Patterson AFB, Ohio

Abstract

An experimental and computational study of boundary layer stability in a hypersonic circular cone flow was made in order to examine the issue of dynamic similarity in the presence of significant changes in the values of the transport properties. The stability of the boundary layer on a 7° sharp cone at freestream Mach 6 was measured at total temperatures of 472 K and 583 K to verify these effects. In both cases the freestream unit Reynolds number was 3.3×10^6 m^{-1} and the model wall temperature was 63% of the total temperature. Increased total temperature stabilizes the boundary layer, as predicted by linear stability theory. Although measured amplification rates show some scatter, integrated disturbance amplitudes agree well with linear stability theory.

Nomenclature

A = disturbance amplitude, nondimensional
a = sound speed, m/s
C_H = nondimensional heat transfer coefficient, $\dot{q} / \rho_e u_e c_p (T_r - T_w)$
c_p = constant pressure specific heat, N m/kg K
f = frequency, kHz
k = thermal conductivity, W/mK
L = model length, 1.016 m
M = Mach number, u/a
N = integrated amplification rate, $\ln(A / A_o)$
Pr = Prandtl number, $\mu C_p / k$
$\dot{q}$ = heat flux, W/m^2
R = $\sqrt{\mathrm{Re}}$
Re = Reynolds number based on boundary layer edge conditions, $\rho_e u_e s / \mu_e$
Re_u = freestream (upstream of model bow shock) unit Reynolds number, m^{-1}
s = running length along cone surface, m
T = temperature
u = velocity component parallel to model surface, m/s
x = length along model longitudinal axis, m
y = coordinate measured normal to model surface, m
α_i = amplification rate, nondimensional
δ = boundary layer velocity thickness, m
γ = adiabatic exponent, nondimensional
η = similarity coordinate, $y\sqrt{\mathrm{Re}} / s$
μ = viscosity, kg/m/s
ρ = density, kg/m^3

Subscripts

e = boundary layer edge conditions
r = recovery temperature
tr = transition
w = wall conditions
0 = stagnation conditions, lower neutral bound location

---

* Aerospace Engineer, Senior Member
† Aerospace Engineer, Member

Introduction

Hypersonic flight improves weapon survivability and response time. Boundary layer transition to turbulence is important to hypersonic vehicle design primarily because turbulence increases heat transfer to the vehicle. Higher heat transfer generally requires higher-performance thermal protection, at the price of increased weight and cost. Transition also impacts engine and aerodynamic performance. Increased drag from turbulent skin friction is important to hypersonic vehicles with large wetted areas and extended flight times. These factors place a premium on understanding transition for prediction and control.

Dynamic similarity, the condition that the dependent variables of two flowfields collapse in nondimensionalized coordinates, is often assumed in analyses of boundary layer stability. In order to achieve exact similarity, all the parameters in the equations of motion, such as local Reynolds number and local Prandtl number, must be the same at corresponding points in the two flows. A mathematical analysis of the equations of motion for a compressible, ideal gas flow shows that, in general, exact dynamical similarity can only exist if the adiabatic exponent, γ, and the Prandtl number are constant, and all the transport properties are proportional to a power of the absolute temperature.[1] Although these conditions are often a useful approximation for air flows, dynamic similarity will not exist for significant changes in total temperature at fixed freestream Mach number and Reynolds number. Mack[2,3] predicted that hypersonic boundary layer stability increases with increasing total temperature, even when wall-to-total-temperature ratios are held constant. This total temperature effect is due to the variation of the air viscosity, thermal conductivity, and specific heat with temperature.[4] This effect is predicted even for inviscid analyses because of the influence of the transport properties on the basic state. Total temperature effects must be accounted for in extrapolating wind tunnel data to free-flight conditions, and they provide a demanding test of base flow computations. Total temperature effects must also be considered in facilities with unsteady stagnation conditions.[5]

Several experiments have suggested that weak ionization of the air upstream of a vehicle may reduce heat transfer. At least one review of the literature on these effects has been compiled.[6] A cautionary note in interpreting these data is that the neutral gas temperature is often elevated when the ionizing discharges are created, and thus will affect the stability characteristics of the boundary layer. The effect of the ionization on the transport properties should also be considered.

Little experimental verification of total temperature effects exists. Experiments on a hollow cylinder[7] appeared to show a slight decrease in transition Reynolds number when total temperature was increased by 44-47%, but these results are difficult to interpret since the tunnel freestream unit Reynolds number also varied.

Experiment

Tests were carried out in the Arnold Engineering Development Center von Karman Gas Dynamics Facility Tunnel B (AEDC VKF-B) to explore total temperature effects. The VKF-B facility and its freestream disturbance levels have been described in previous references.[8,9] Tests were carried out at a freestream Mach number of 5.96 and at total temperatures of 472 K (low T_0 case) and 583 K (high T_0 case). If a linear variation of air viscosity with temperature is assumed, it is easy to derive the useful rule of thumb that freestream unit Reynolds number varies as the –3/2 power in total temperature for constant stagnation pressure. The tunnel stagnation pressure was varied from 3.69×10^5 Pa for the low T_0 case to 5.07×10^5 Pa for the high T_0 case to maintain a constant freestream (upstream of the model shock) unit Reynolds number of 3.3×10^6 m^{-1}. The measured boundary layer edge unit Reynolds number was 4.13×10^6 m^{-1}.

The windtunnel model was previously used to explore wall-temperature effects[10,11], and Mach number effects.[12] The model was a sharp-nosed (50 μm radius), 1.016 m long cone with half-angle of 7°. The cooled portion of the model (aft 0.875 m) consisted of concentric 6061-T6 aluminum frusta. The outer shell was 3.2 mm thick to

within 5 mm of the forward end of the frustum. Cooling water circulated between the two shells to maintain a constant wall temperature. The solid, uncooled nose of the model was 0.141 m long and constructed of 13-8 stainless steel. A Micarta™ insulating washer 1.6 mm thick separated the uncooled nose from the cooled frustum.

It is well known that wall-cooling destabilizes the second mode, the dominant boundary layer instability over much of the hypersonic flight range.[4] To exclude this effect, a heat exchanger was added to the cooling circuit to maintain the wall temperature at $T_w/T_0 = 0.63$ when total temperature was raised from 472K to 583K. A limited number of heat transfer measurements were also made at $T_w/T_0 = 0.42$.

Surface instrumentation consisted of four static pressure orifices and eight Schmidt-Boelter[13] heat transfer gauges. Measurements in this facility using Schmidt-Boelter gauges[14] showed an accuracy of +/- 10% in measured heat transfer. The heat transfer gauges were arrayed along a ray of the model (zero deg. ray) from $x/L = 0.35$ to $x/L = 0.95$. The pressure taps were spaced around the circumference of the model at 90 deg. intervals, starting at the zero deg. ray, at $x/L = 0.975$. All surveys were made along the top ray of the model. All measurements were made with the model rolled –45 deg. This placed the zero deg. ray 45 deg. from the top on the left-hand side of the model, as viewed from the back of the model looking upstream.

Boundary layer stability is sensitive to model angle of attack.[14,21] The model pressures were monitored to assess any asymmetries. Differential pressures between taps on the top and bottom were less than 1%. Differential pressures between taps on the sides of the model were, on average 1.7% higher on the left. The stated pressure measurement accuracy is 1.3% A 1.7% increase would correspond to a yaw angle of approximately 0.1 to 0.2 deg.

Flowfield probe measurements consisted of hot wire anemometer surveys and mean-flow boundary layer profiles. The instrumentation is described in detail in previous publications.[15] Hot wire measurements were made by traversing the hot wire vertically through the boundary layer at each x-location while the broadband rms output of the wire was recorded. The point in the boundary layer where the broadband rms voltage fluctuations peaked is termed the maximum energy location, and all measurements were made at this height. Measurements were taken at 25.4 mm intervals in the streamwise direction.

Hot wire measurements were made with uncalibrated hot wires. Fluctuating voltages obtained with uncalibrated wires cannot be converted into velocity and thermodynamic fluctuations. However, since the local Reynolds number is essentially constant at the maximum energy location, the wire sensitivity is constant at all measuring stations. Variations in the fluctuating voltage amplitudes from one x-station relative to another thus represent the same relative changes in the fluid fluctuations. Linear theory assumes that all velocity components and thermodynamic quantities have identical amplification rates. Previous measurements[11] show this to be true in the linear regime. Amplification rates and N-factors based on raw hot-wire voltages are thus representative of disturbance amplification rates and N-factors.

Computations

The linear cone boundary layer stability was computed using the e^{Malik} code.[24] The boundary layer basic state for the linear stability analysis was computed using the built-in similarity solver in the e^{Malik} code, with constant $Pr = 0.72$, and $c_p = 1004.5$ N m / kg K . Since Pr and c_p were held constant, total temperature effects enter the basic state and stability calculations through the viscosity variation. It should be noted that a distinction is made between dynamic similarity, as defined in the introduction, and self-similar boundary layer profiles. N-factors were calculated by using the program option which maximizes growth rate at each x-station, allowing wave angle to vary. Since the wall cooling stabilized the first mode at the frequencies and Reynolds numbers computed, all growth was confined to second mode disturbances, and the maximum growth always occurred at zero wave angle.

A boundary layer similarity solver was written in-house in order to more fully explore the basic state profiles. This program used the formulation of Mack.[16] Transport properties were modeled using constant Pr = 0.72, c_p = 1004.5 N m / kg K, and Sutherland viscosity to 110K, with linear variation below this temperature. Results were transformed to the cone using the Mangler transformation. The program gave results identical to the e^{Malik} basic state solver.

To examine the effect of the hot nosetip, a finite-difference code was also written to calculate the boundary layer for a non-isothermal wall. A step change in wall conditions was imposed at x/L = 0.139. This program used the same transport property modeling as the similarity solver. An implicit formulation with lagged coefficients was used. This code was validated by comparing constant-temperature wall results to output from the two similarity solvers.

Results

Non-Isothermal Wall Effects

The effect of non-isothermal wall conditions created by the uncooled nosetip were of some concern. It should be noted that this condition is common in cooled wind tunnel models. Two steps were taken to assess uncooled-nose effects.

The first step was to rapidly inject the model and record heat transfer while the nosetip and frustum were both at ambient temperature (300 K), then at one-minute intervals as the nosetip heated. These tests were carried out at T_0 = 720 K (T_w/T_0 = 0.42) and $Re_u = 3.3\text{x}10^6$ m^{-1} to match AEDC VKF-B Mach 8 cold wall conditions and obtain the maximum disparity between nose and frustum temperatures. The TOPAZ[17] finite-volume transient heat transfer code was used to estimate the nose temperature. Results show that for the hot case, the downstream (and coolest) portion of the nose surface had reached 76% of equilibrium temperature 10 minutes after model injection. The results in Fig. 1 show an increase in heat transfer to the frustum when the nosetip is hot, as expected, but there is very little change in transition location. Experiments by Kendall[18] on a 10 deg. cone at Mach 4.1 also showed similar results.

The second step was to compute the boundary layer basic state using the finite difference code with a step change in wall conditions at the end of the nose. These results showed that by x/L = 0.175 (R = 857), the peak temperature in the boundary layer had relaxed to within 5% of the peak temperature in the isothermal wall boundary layer. Gasperas[19] computed the basic state and linear stability of a flat plate boundary layer with an adiabatic leading edge. Conditions for this computation matched edge conditions for a 7-deg. sharp-nose cone in AEDC VKF-B at freestream Mach 8. The wall condition was adiabatic over the first 0.0428 m of the plate. The remainder of the plate was held at 42% T_0. The basic state calculations showed that 0.171 m downstream of the change in wall conditions, the peak temperature in the boundary layer was approximately 5% higher than the peak temperature in the isothermal wall boundary layer. The hot leading edge stabilized the boundary layer immediately downstream, but farther downstream the stability characteristics approached those of the isothermal wall boundary layer. Non-isothermal wall effects would be greater in this computational case than in the current experiment, since the wall is more highly cooled in the computation.

In summary, the hot nosetip is not expected to greatly affect the boundary layer stability characteristics in the present experiment. The boundary layer profiles have largely relaxed to isothermal wall profiles by x/L=0.275, or R=1075. Frequencies leading to transition in the current experiment do not begin to amplify until R=1300 (see section on Linear Stability). Also, the hot nosetip had no significant effect on the transition location for T_w/T_0 = 0.42.

Mean Measurements

Fig. 2 shows mean heat transfer. Predicted laminar heat transfer from a boundary layer similarity solution with an isothermal wall is shown for comparison. Heat transfer for the non-isothermal wall was calculated using the

finite-difference boundary layer code, and these results are also shown in Fig. 2.

The transition location is defined in this paper as the location where heat transfer first rises above laminar values. This point was determined by fairing a straight line through the two most downstream data points and determining where this line intersected the similarity solutions for laminar heat transfer. Transition occurs at approximately $Re = 3.6\text{x}10^6$ for the hot case, compared to $3.3\text{x}10^6$ for the cold case, indicating the stabilizing effect of increased total temperature.

Mean profiles of total temperature and pitot pressure were measured at nominal x/L locations of 0.275, 0.425, and 0.675. Mach number profiles derived from these measurements are plotted in Fig. 3. The x/L=0.675 measurements agree well with computed similarity profiles, even showing the slight thickening of the boundary layer with lower T_0, as predicted. However, near the nose, the measured profiles drift upward. At x/L=0.275, the measured profiles more closely resemble an adiabatic boundary layer than the cooled wall boundary layer. The hot nosetip was suspected as a cause of this discrepancy. Calculations for the non-isothermal wall boundary layer, however, show that by x/L = 0.275 the boundary layer has largely relaxed to the cooled wall similarity profiles. The most likely cause of the upward drift in the boundary layer profiles is a systematic error in the measured y-location.

The boundary layer stability parameter, $d(\rho du/dy)/dy$, was derived from the isothermal wall similarity solution. The results, in Fig. 4, show two inflection points in $\rho du/dy$ (the zero-crossings in Fig. 4). The inflection point for the low T_0 case occurs higher in the boundary layer than the high T_0 case. Mack relates this behavior in the generalized inflection point to decreased boundary layer stability, in analogy to the velocity inflection point in the subsonic Falkner-Skan boundary layer.[20] As the unfavorable pressure gradient in the Falkner-Skan boundary layer increases, the inflection point moves away from the wall, and this is correlated with increasing instability.

Power Spectra

Power spectra for the high and low T_0 cases are shown in Figs. 5 and 6. Both cases show behavior typical of the cooled cone at Mach 8.[10] The spectra are strikingly similar to those measured in the NASA Langley Mach 6 quiet tunnel on a flared cone.[21,22] The prominent spectral peak between approximately 100 and 140 kHz has previously been identified as the second mode.[11] Little first mode amplification is evident due to the wall-cooling. The spectral peak at twice the second mode frequency corresponds to a nonlinear harmonic of the second mode.[23] In both cases, the second mode frequency decreases as Reynolds number increases. This is because the peak second mode frequency is approximately $u_e/2\delta$.[11] Interestingly, the peak second mode frequency for the cold case is approximately 90% of the hot case peak second mode frequency. This is due to the change in velocity between the two cases. Since the Mach number is equal for the two cases, the velocity will go as the sound speed, or the square root of the total temperature. Since in most facilities, as in free flight, the spectrum of the background disturbances depends on frequency, the initial amplitudes of disturbances will thus vary with total temperature and should be considered. The decreased boundary layer stability for the cold total temperature is reflected in the earlier rise of the second mode above background disturbance levels.

Linear Stability

Measured disturbance growth near the peak second mode frequencies was compared to computed results from the e^{Malik} linear stability code.[24] Results are shown in Figs. 7 and 8. Experimental amplification rates were determined by fitting a fourth-order, least-squares polynomial to the measured disturbance amplitudes at each frequency. The amplification rate is then determined by taking the derivative of the polynomial, dA/dR, and normalizing this by the local amplitude. Near the peak amplification location, linear stability theory agrees with the measured amplification rates to within about 20%. Considering the uncertainty associated with taking derivatives of

experimental data, this level of disagreement is probably within the experimental uncertainty. Agreement between experiment and computation is very poor near the beginning and end measuring stations. At these stations, the disturbance amplitude and signal-to-noise ratio are generally low. Since the end derivatives of the curvefits are not specified, they have a tendency to "curl up" and produce large amplification rates.

Since the measured amplification rates are subject to such uncertainty, the integrated amplitudes were examined by comparing computed to measured N-factors. The principal difficulty in determining N-factors experimentally is the choice of A_0 to normalize amplitudes. The initial amplitudes are generally low and subject to experimental scatter, and the experimental lower neutral bound is difficult to ascertain. Small changes in A_0 can produce large changes in N-factor. As an objective approach, the measured disturbance amplitudes were interpolated to the computed lower neutral bound location using sixth-order polynomials, and this amplitude was used as A_0 for the experimental data. A sixth-order polynomial fit was chosen over the fourth-order fit, since the sixth-order polynomial oscillated less near the lower neutral bound. The results, in Figs. 9 and 10, show generally a good agreement between the measured and computed N-factors until near the computed upper neutral bound. The integrated effect of amplification rate errors at lower Reynolds number are inconsequential since the amplification rates and amplitudes are small.

A more significant discrepancy is that the experiments show continued disturbance growth beyond the computed upper neutral bound and attain higher N-factors than the computation. This disagreement may reflect nonlinear effects occurring at higher amplitude.

Computed N-factor envelopes for both cases are shown in Figs. 11 and 12. Previous studies[2] have shown that an N-factor of approximately 4 correlates transition on axisymmetric cones in AEDC VKF-B at Mach 8. The $N = 4$ locations for the low and high T_0 cases are R = 1818 and 1900 ($Re = 3.3\text{x}10^6$ and $3.6\text{x}10^6$), respectively), which correlate with the measured transition locations.

Conclusions

An experimental and computational study of boundary layer stability in a Mach 6 flow over a 7-degree circular cone was made in order to examine the issue of dynamic similarity in the presence of significant changes in the values of the transport properties. An assumption of dynamic similarity is often a useful approximation for reducing data, but exact dynamic similarity can only exist in an ideal gas flow if γ and Pr are constant, and all the transport properties follow power laws in the absolute temperature. In the present work, significant changes in boundary layer stability were observed for different values of the total temperature when the Mach number, Reynolds number, and ratio of wall to freestream temperature were held constant. Increasing total temperature by 24% at freestream Mach 6 stabilizes the boundary layer and increases the length of laminar flow approximately 10%. Scatter in the experimental data make it difficult to reliably extract amplification rates, but integrated growth rates show good agreement with computation. Linear stability calculations predict N-factors well at lower Reynolds number, but underpredict maximum N-factor.

The presence of a hot nosetip on the model had little effect on boundary layer stability and transition for these conditions. The boundary layer quickly relaxes to isothermal wall profiles downstream of the change in wall conditions. Efforts to utilize non-uniform wall cooling for transition control would be more effective if concentrated near the lower neutral bound of the "most dangerous" disturbance frequencies.

Acknowledgments

This experiment was originally conceived by Ken Stetson, formerly of the Air Force Wright Laboratory. It was carried out under a basic research laboratory task monitored at the time by Len Sakell of the Air Force Office of Scientific Research, currently monitored by Steven Walker. The AEDC test engineer was Joseph Donaldson, formerly of Calspan Corp., AEDC

Operations. The authors wish to thank Charles Nelson of Sverdrup Technologies and the rest of the AEDC team for conducting tunnel operations.

References

[1] Serrin, J., "Mathematical Principles of Classical Fluid Mechanics," *Handbuch der Physik*, vol. 8, pp. 243-246, Springer-Verlag, 1959.

[2] Mack, L. M., "Boundary-Layer Stability Analysis for Sharp Cones at Zero Angle-of-Attack," Air Force Wright Aeronautical Laboratory Technical Report AFWAL-TR-86-3022, Wright-Patterson AFB, Aug. 1986.

[3] Mack, L. M., "Stability of Axisymmetric Boundary Layers on Sharp Cones at Hypersonic Mach Numbers," AIAA-87-1413, Jun. 1987.

[4] Mack, L. M., "On the Inviscid Acoustic-Mode Instability of Supersonic Shear Flows Part 1: Two-Dimensional Waves," *Theoretical and Computational Fluid Dynamics*, vol. 2, 1990, pp. 97-123.

[5] Schneider, S. P., Haven, C. E., McGuire, J. B., Collicott, S. H., Ladoon, D., and Randall, L. A., "High-Speed Laminar-Turbulent Transition Research in the Purdue Quiet-Flow Ludwieg Tube," AIAA 94-2504, June, 1994.

[6] Adamovich, I. V. , Subramaniam, V. V., Rich, J. W. , and Macheret, S. O. "Phenomenological Analysis of Shock-Wave Propagation in Weakly Ionized Plasmas", *AIAA J.* vol. 36, no. 5, May 1998, pp. 816-822.

[7] Ross, R., "Influence of Total Temperature on Transition in Supersonic Flow," *AIAA J.*, vol. 11, no. 4, Apr. 1973, pp. 563-565.

[8] Boudreau, A. H., "Performance and Operational Characteristics of AEDC/VKF Tunnels A, B, and C," Arnold Engineering Development Center Technical Report AEDC-TR-80-48 (AD A102614), Arnold AFS, July 1981.

[9] Donaldson, J. and Coulter, S., "A Review of Free-Stream Flow Fluctuation and Steady-State Flow Quality Measurements in the AEDC/VKF Supersonic Tunnel A and Hypersonic Tunnel B," AIAA 95-6137, Apr. 1995.

[10] Stetson, K. F., Thompson, E. R., Donaldson, J. C., and Siler, L. G., "Laminar Boundary Layer Stability Experiments on a Cone at Mach 8, Part 5: Tests with a Cooled Model, AIAA 89-1895, Jun. 1989.

[11] Stetson, K. F., and Kimmel, R. L., "On Hypersonic Boundary-Layer Stability, " AIAA 92-0737, Jan. 1992.

[12] Stetson, K. F., and Kimmel, R. L., "Example of Second-Mode Instability Dominance at a Mach Number of 5.2," *AIAA J.*, vol. 30, no. 12, Dec. 1992, pp. 2974-2976.

[13] Kimmel, R. L., and Poggie, J., "Transition on an Elliptic Cone at Mach 8," American Society of Mechanical Engineers ASME FEDSM97-3111, Jun. 1997.

[14] Kimmel, 1993, "Experimental Transition Zone Lengths in Pressure Gradient in Hypersonic Flow," American Society of Mechanical Engineers ASME FED Vol. 151, Symposium on Transitional and Turbulent Compressible Flows, Jun. 1993, pp. 117-127.

[15] Stetson, K. F., Thompson, E. R., Donaldson, J. C., and Siler, L. G., "Laminar Boundary Layer Stability Experiments on a Cone at Mach 8, Part 1: Sharp Cone," AIAA 83-1761, Jul. 1983.

[16] Mack, L. M., "Computation of the Stability of the Laminar Compressible Boundary Layer," *Methods in Computational Physics*, vol. 4, edited by Alder, B., Fernbach, S., and Rotenberg, M., pp. 247-299, Academic Press, New York, 1965.

[17] Beck, J. V., Tu, J. S., "IHCP2D: Computer Program for Solutions of General Two-Dimensional Inverse Heat Conduction Problems," Air Force Wright Aeronautical Laboratory Technical Report AFWAL-TR-88-3111, Wright-Patterson AFB, Ohio, Mar. 1989.

[18] Kendall, J. M., "Wind Tunnel Experiments Relating to Supersonic and Hypersonic Boundary-Layer Transition," AIAA 74-133, Jan. 1974.

[19] Gasperas, G., "Effect of Wall Temperature Distribution on the Stability of the Compressible Boundary Layer," AIAA 89-1894, Jun. 1989.

[20] Mack, L. M., "Boundary-Layer Stability Theory," *Special Course on Stability and Transition of Laminar Flow*, edited by R. Michel, AGARD Report No. 709, pp. 3-1 to 3-81, 1984.

[21] Lachowicz, J. T., Chokani, N., and Wilkinson, S. P., "Boundary-Layer Stability Measurements in a Hypersonic Quiet Tunnel," *AIAA J.*, vol. 34, no. 12, Dec. 1996, pp. 2496-2500.

[22] Doggett, G. P., Chokani, N., and Wilkinson, S. P., "Effect of Angle of Attack on Hypersonic Boundary-Layer Stability," *AIAA J.*, vol. 35, no. 3, Mar. 1997, pp. 464-470.

[23] Kimmel, R. L., and Kendall, J. M., "Nonlinear Disturbances In a Hypersonic Laminar Boundary Layer," AIAA 91-0320, Jan. 1991.

[24] Malik, M. R., "e^{Malik}: A New Spatial Stability Analysis Program for Transition Prediction Using the e^N Method," High Technology Corporation Report No. HTC-8902, March 1989.

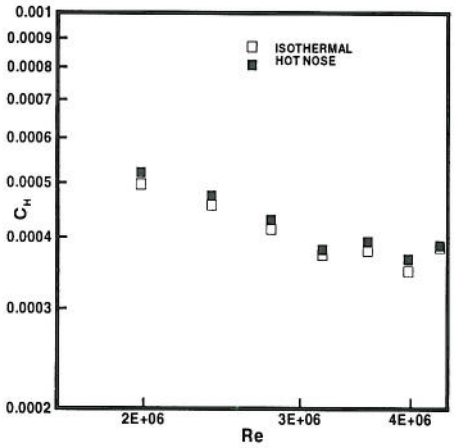

Figure 1. Effect of hot nosetip on heat transfer.

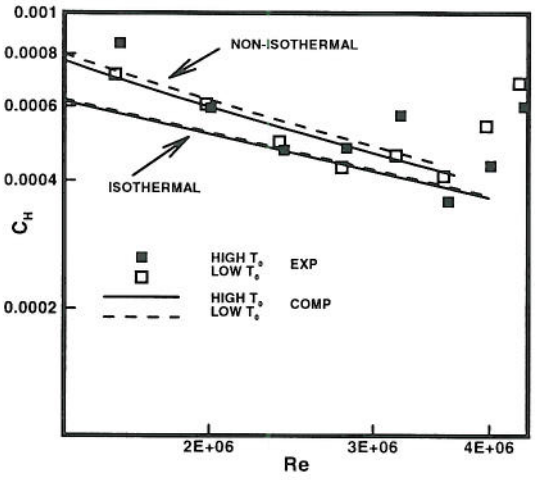

Figure 2. Heat transfer for high and low total temperature cases.

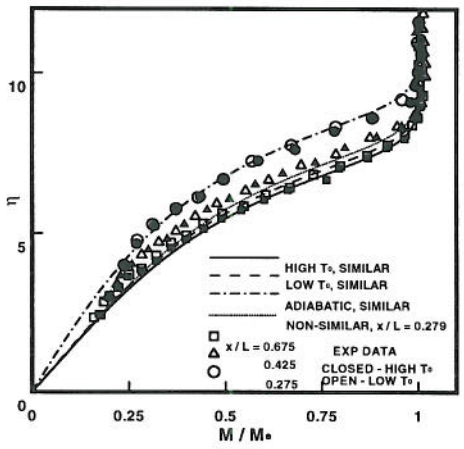

Figure 3. Profiles of mean Mach number.

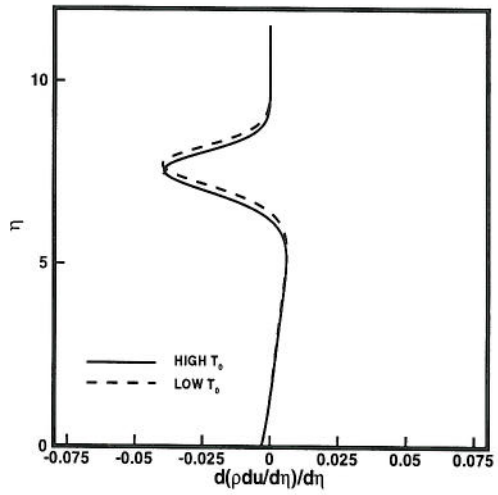

Figure 4. Profiles of stability parameter.

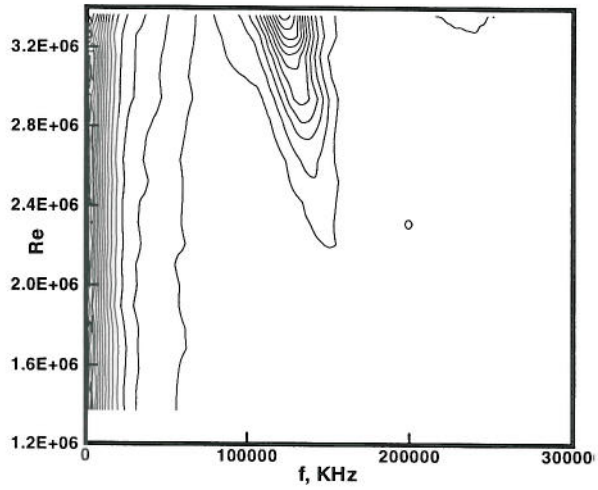

Figure 5. Contours of power spectral density for high total temperature case.

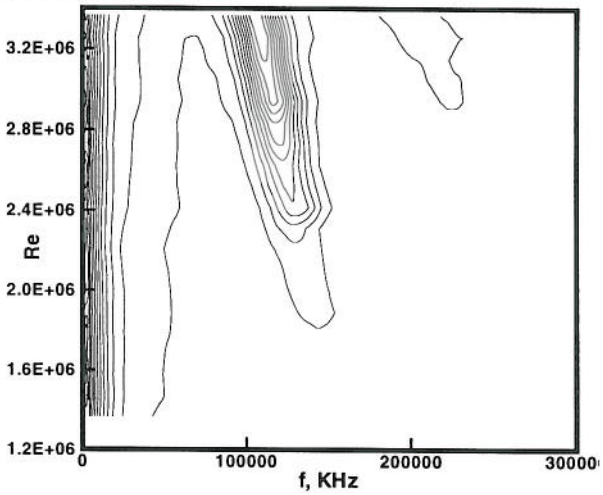

Figure 6. Contours of power spectral density for low total temperature case.

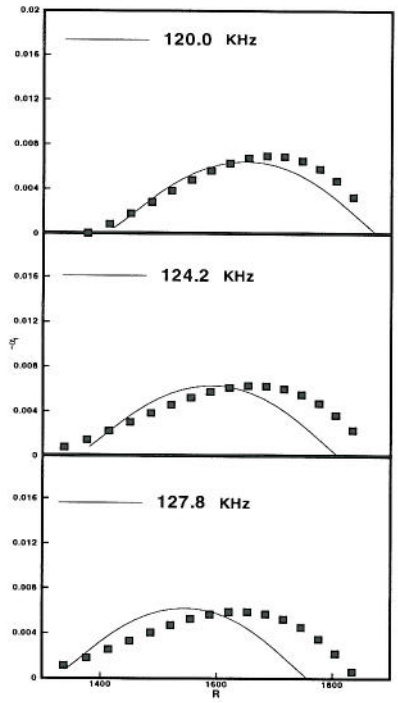

Figure 7. Measured and computed amplification rates for high T_0 case.

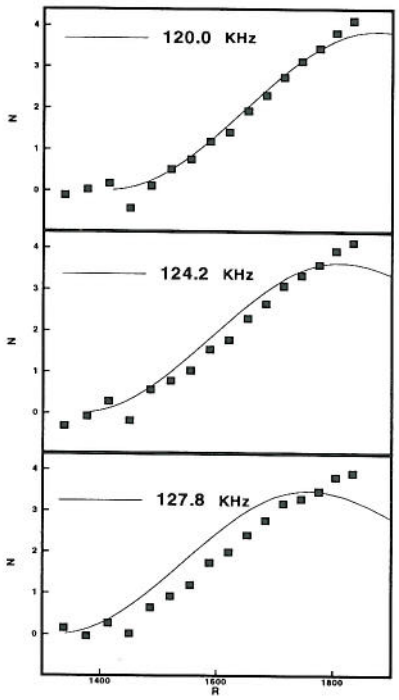

Figure 9. Measured and computed N-factors for high T_0 case.

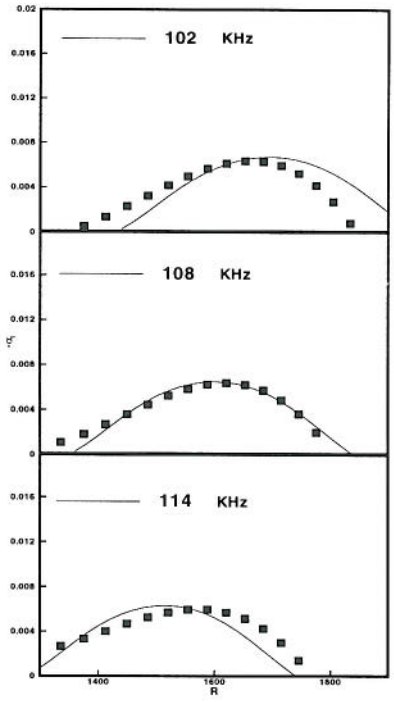

Figure 8. Measured and computed amplification rates for low T_0 case.

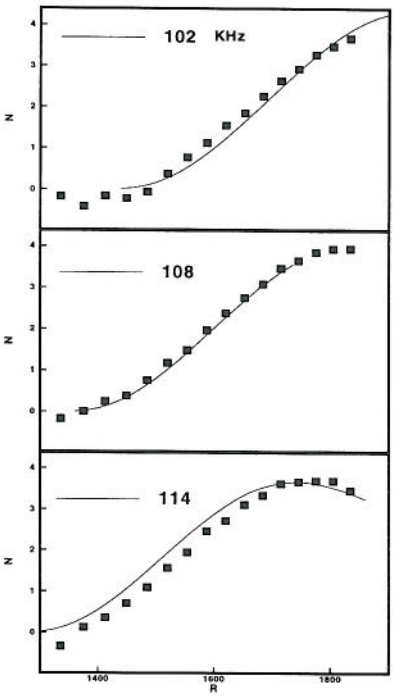

Figure 10. Measured and computed N-factors for low T_0 case.

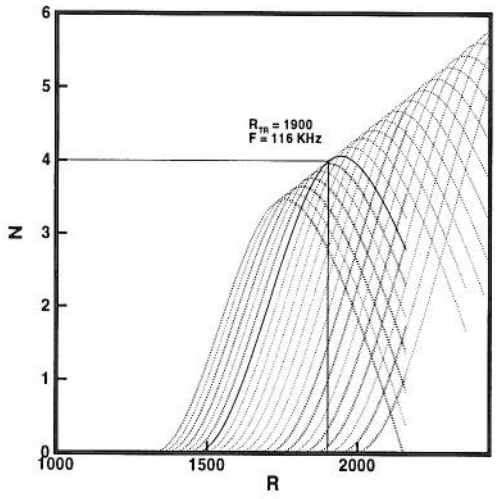

Figure 11. N-factor envelope for high T_0 case.

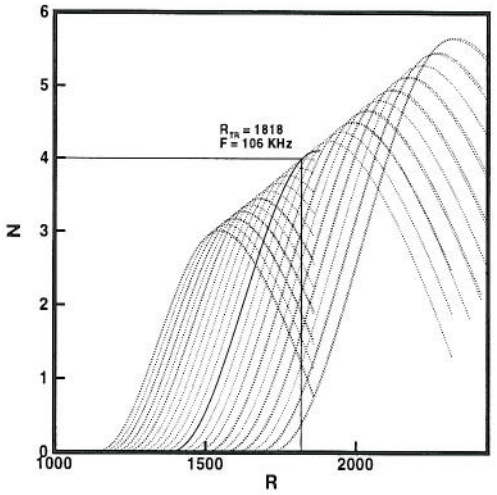

Figure 12. N-factor envelope for low T_0 case.